Dating the rise of atmospheric oxygen

A. Bekker[1], H. D. Holland[1], P.-L. Wang[2], D. Rumble III[2], H. J. Stein[3], J. L. Hannah[3], L. L. Coetzee[4] & N. J. Beukes[4]

[1]*Department of Earth and Planetary Sciences, 20 Oxford Street, Harvard University, Cambridge, Massachusetts 02138, USA*
[2]*Geophysical Laboratory, Carnegie Institution of Washington, 5251 Broad Branch Road, Washington DC 20015, USA*
[3]*AIRIE Program, Department of Geosciences, Colorado State University, Fort Collins, Colorado 80523-1482, USA*
[4]*Department of Geology, Rand Afrikaans University, Auckland Park 2006, Johannesburg, South Africa*

Several lines of geological and geochemical evidence indicate that the level of atmospheric oxygen was extremely low before 2.45 billion years (Gyr) ago, and that it had reached considerable levels by 2.22 Gyr ago. Here we present evidence that the rise of atmospheric oxygen had occurred by 2.32 Gyr ago. We found that syngenetic pyrite is present in organic-rich shales of the 2.32-Gyr-old Rooihoogte and Timeball Hill formations, South Africa. The range of the isotopic composition of sulphur in this pyrite is large and shows no evidence of mass-independent fractionation, indicating that atmospheric oxygen was present at significant levels (that is, greater than 10^{-5} times that of the present atmospheric level) during the deposition of these units. The presence of rounded pebbles of sideritic iron formation at the base of the Rooihoogte Formation and an extensive and thick ironstone layer consisting of haematitic pisolites and oölites in the upper Timeball Hill Formation indicate that atmospheric oxygen rose significantly, perhaps for the first time, during the deposition of the Rooihoogte and Timeball Hill formations. These units were deposited between what are probably the second and third of the three Palaeoproterozoic glacial events.

It was proposed long ago that the redox state of the atmosphere changed during the early Palaeoproterozoic[1]. Sedimentary successions of age ≥2.45 Gyr include placer deposits that contain detrital uraninite, siderite and pyrite[2,3], reduced shallow-water facies of iron formations[4], highly carbonaceous shales that are not enriched in redox-sensitive elements[5,6] and palaeosols that are not oxidized[6]. Early diagenetic pyrite in these successions has $\delta^{34}S$ values consistent with a seawater sulphate content of <200 μM (ref. 7; see Table 1 for a definition of δ notation). In contrast, sedimentary successions younger than 2.22 Gyr contain red beds[8], $CaSO_4$-rich evaporites[9,10], and shallow-water iron formations that are oxidized[11]. These successions overlie oxidized palaeosols[12] and have $\delta^{34}S$ records that are consistent with seawater sulphate concentrations >200 μM (ref. 13). The changes are strong evidence for a major increase in the O_2 content of the atmosphere between 2.45 and 2.22 Gyr ago, although it has been argued that they are related to differences in post-depositional alteration and to different tectonic settings rather than to an increase in the level of atmospheric oxygen[14–17].

The recent discovery of mass independent fractionation (MIF) in sulphur isotopes has provided a new tool for tracing changes in the oxygen content of the atmosphere[18]. Sulphur of sulphides and sulphates from sedimentary units older than 2.47 Gyr has values of MIF (expressed in terms of $\Delta^{33}S$; see Table 1 for a definition of Δ notation) ranging from −2.5‰ to +8.1‰, whereas all sulphides and sulphates younger than 1.9 Gyr have $\Delta^{33}S$ values <|0.4‰| (refs 18–20). The only known mechanism for producing MIF in sulphur isotopes is photodissociation in the gas phase[21], which has been observed in the modern atmosphere[22]. Preservation of large MIF signals in the Archaean record is probably related to the lack of an ozone shield in the atmosphere, allowing deep penetration of high energy ultraviolet and photochemical dissociation of SO_2 into elemental and water-soluble S species. The isotopic composition of elemental sulphur particles and water-soluble S species did not exchange completely in the Archaean atmosphere; hence some of their MIF signal was delivered to the Earth's surface[23]. In an atmosphere with an oxygen content larger than $\sim 10^{-5}$ times the present atmospheric level (PAL)[23], sulphur species are oxidized to sulphate, exchange, and lose most of their MIF signal. The change from an anoxic to an oxygenated atmosphere therefore explains the absence of $\Delta^{33}S$ values >0.4‰ in the S isotopes of sulphides and sulphates during the past 1.9 Gyr, a period during which the atmospheric partial pressure of oxygen (p_{O_2}) has been much greater than 10^{-5} PAL. These observations suggest that it should be possible to determine when p_{O_2} became $>10^{-5}$ PAL by defining the time when the range of MIF signals in sedimentary sulphides and sulphates decreased to <0.4‰. The results of our study of synsedimentary to early diagenetic pyrites in black shales of South Africa suggest that by 2.32 Gyr ago atmospheric p_{O_2} was already $>10^{-5}$ PAL.

Geological setting of studied units

The Rooihoogte Formation and the conformably overlying Timeball Hill Formation of the Pretoria Group, South Africa (Figs 1 and

Table 1 **Sulphur isotope data and stratigraphic position of samples**

Number	GC	$\delta^{34}S$ (‰)	$\delta^{33}S$ (‰)	$\delta^{34}S^*$ (‰)	$\delta^{33}S^*$ (‰)	$\Delta^{33}S_{In}$ (‰)	Depth (m)
Timeball Hill Formation							
EBA2/30-1	c	−25.56	−13.13	−25.89	−13.22	0.08	1,333.0–1,333.1
-2	c	−26.23	−13.51	−26.58	−13.60	0.04	1,333.0–1,333.1
-3	c	−25.6	−13.16	−25.93	−13.25	0.07	1,333.0–1,333.1
EBA2/34-1	d	−31.07	−16.18	−31.56	−16.31	−0.11	1,333.4–1,333.5
-2	c	−34.69	−17.93	−35.31	−18.09	0.03	1,333.4–1,333.5
-3	c	−33.28	−17.2	−33.85	−17.35	0.03	1,333.4–1,333.5
-4	d	−33.39	−17.12	−33.96	−17.27	0.17	1,333.4–1,333.5
-5	c	−33.45	−17.31	−34.02	−17.46	0.00	1,333.4–1,333.5
EBA2/38-1	d	−31.06	−16.18	−31.55	−16.31	−0.11	1,333.8–1,333.9
-2	d	−32.59	−17.02	−33.13	−17.17	−0.16	1,333.8–1,333.9
Rooihoogte Formation							
EBA2/67-1	d	−29.88	−15.59	−30.34	−15.71	−0.14	1,335.48–1,335.68
-2	c	−26.92	−13.78	−27.29	−13.88	0.13	1,335.48–1,335.68
-3	d	−23.91	−12.22	−24.20	−12.30	0.13	1,335.48–1,335.68
-4	d	−25.34	−12.82	−25.67	−12.90	0.27	1,335.48–1,335.68
EBA2/55-1	d	−29.07	−14.87	−29.50	−14.98	0.16	1,335.65–1,335.85
-2	d	−29.58	−15.29	−30.03	−15.41	0.01	1,335.65–1,335.85
EBA2/59-1	d	−25.76	−13.06	−26.10	−13.15	0.25	1,336.37–1,336.55
-2	d	−25.46	−12.83	−25.79	−12.91	0.33	1,336.37–1,336.55
EBA2/60-1	d	−28.92	−14.83	−29.35	−14.94	0.12	1,336.55–1,336.62
-2	c	−29.98	−15.45	−30.44	−15.57	0.06	1,336.55–1,336.62

In column GC (gas chromatograph record): c, clean (no significant peaks other than SF_6 were seen); d, dirty (peaks in addition to SF_6 were seen; the impurities were vented and did not enter the ion source of the mass spectrometer). Sulphur isotope ratios are represented by conventional δ notation with respect to CDT as $\delta^x S = 1{,}000[(^xS/^{32}S)_{sample}/(^xS/^{32}S)_{CDT} - 1]$, where x is either 33 or 34. $\Delta^{33}S$ is defined by the following equation: $\Delta^{33}S = \delta^{33}S - (0.5138\delta^{34}S)$. The accuracy and precision of the technique as determined by repeated KrF excimer laser analyses of isotopically homogeneous sphalerite from Broken Hill, Australia, and comparison with CO_2 laser analyses of powders microdrilled adjacent to *in situ* analyses, is better than 0.2‰ (1σ) for both $\delta^{33}S$ and $\delta^{34}S$, while values of $\Delta^{33}S$ are measured to ±0.07‰ (ref. 33). Several grains or different spots of the same grain were analysed in each sample; these are marked with a numerical extension after the sample number (for example, -1; -2; -3; and so on). Depths are given as m below surface.

©2004 Nature Publishing Group

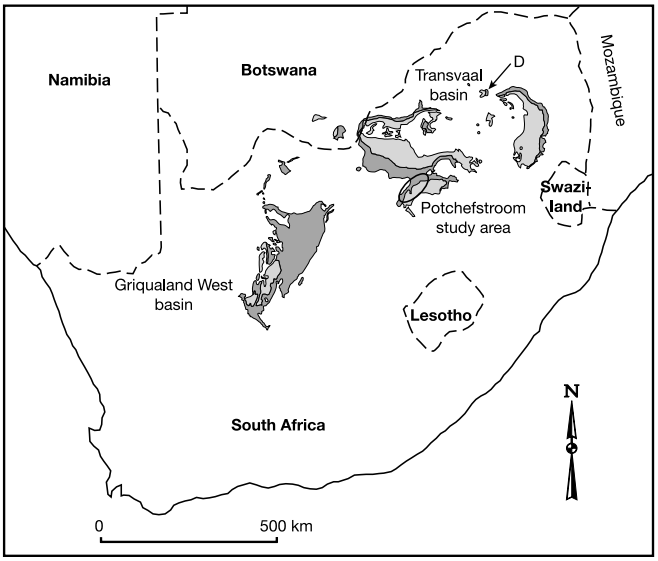

Figure 1 Map of Early Palaeoproterozoic sedimentary successions of South Africa. Distribution of the Chuniespoort (dark grey) and Pretoria (light grey) groups in the Transvaal structural basin and Ghaap (dark grey) and Postmasburg (light grey) groups in the Griqualand West structural basin of South Africa (after Coetzee[28]). Both structural basins belong to the same depositional basin. 'D' indicates the location of the Duitschland Formation exposures.

2) overlie a prominent karstified unconformity on the Late Archaean Malmani carbonate platform and the 2,480 ± 6-Myr-old Penge Iron Formation[24]. Several lines of evidence suggest that the units below the unconformity are older than the rise of atmospheric oxygen: (1) early diagenetic pyrite of the Gamohaan Formation in the Campbellrand Subgroup carries a strong MIF signal[18]; (2) shallow-water iron formations of the Griqualand West basin, which are slightly younger than the Penge iron formation, are reduced and lack a Ce anomaly[4,25]; (3) $\delta^{34}S$ values of early diagenetic pyrites from these units cluster close to 0‰ and have a narrow range[13,26]; (4) detrital uraninite and pyrite grains are present in the Black Reef Quartzite[3]. Unfortunately, the units immediately below the unconformity in the Transvaal basin (Penge Iron Formation and Tongwane Formation) lack pyrite that is suitable for MIF analysis.

On the basis of stacking patterns, the isopach map, facies analysis, and sedimentary structures, it follows that the Rooihoogte and Timeball Hill formations were deposited in a deltaic part of a basin open to the ocean on the southwest[27–30]. Volcanic contributions to these units are lacking except in the extreme southwestern part of the basin, where the 30-m-thick Bushy Bend Lava occurs within the upper Rooihoogte Formation[28]. The formations are sandwiched between two glacial diamictites, one at the base of the Rooihoogte Formation[28], the other at the top of the Timeball Hill Formation[28,31]. We sampled a 3.6-m-thick section of highly carbonaceous shale that straddles the upper Rooihoogte and lower Timeball Hill formations in core EBA-2. The Rooihoogte Formation is condensed in this area, and the sampled section is only 12.5 m above the base of the formation. The units have been affected by lower greenschist facies metamorphism[28].

Description of the studied material

Pyrite in this section is confined to highly organic-rich layers. It occurs as nodules, mineralized microbial mats, disseminated grains, and laminated seams up to several centimetres in thickness. The nodules are up to several centimetres in diameter. They either have no internal structure or are composed of globules, concentrically laminated, fine-grained pyrite, or radial, bladed pyrite crystals. Where nodules with radial, bladed crystals (spherulites) are closely packed, they form a substrate for layers of fibrous pyrite crystals. The spherulites (Fig. 3) probably consisted initially of marcasite. The small pyrite globules have a diameter of 10–600 μm. The outer parts of the nodules are commonly overgrown by euhedral pyrite crystals. Laminae in the shale bend around nodules, suggesting that

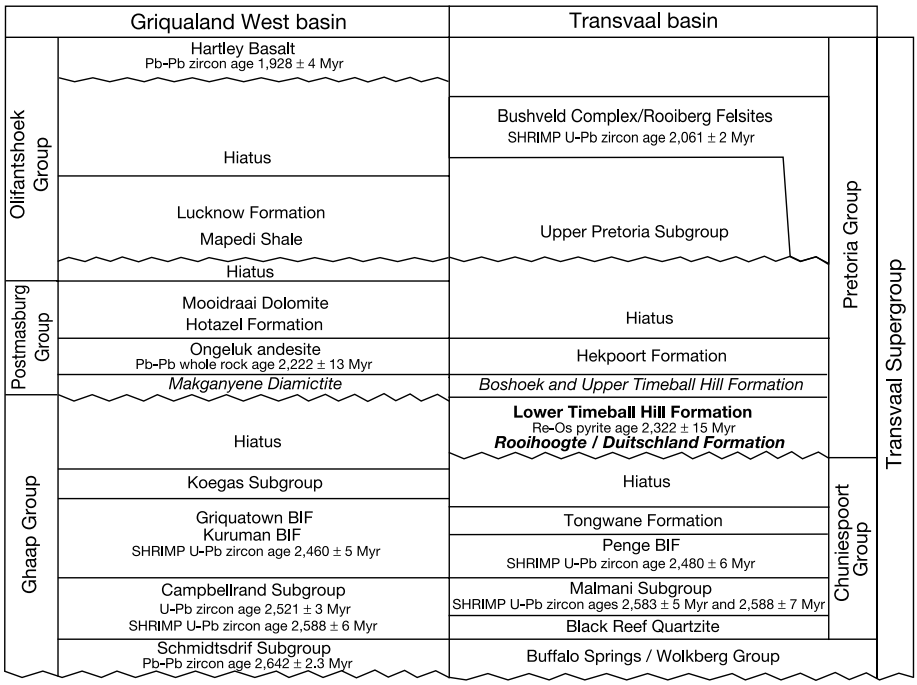

Figure 2 Correlation chart for the Transvaal Supergroup in the Griqualand West and Transvaal structural basins, South Africa (modified from ref. 39). Studied units are shown in bold; units in italics contain glacial diamictites. The Re–Os pyrite age is from ref. 38, the age of the Kuruman iron formation is from ref. 44; see ref. 39 for references to other ages. BIF, banded iron formation; SHRIMP, sensitive high-resolution ion micro-probe.

©2004 Nature Publishing Group

the nodules predate compaction. Microbial mats and microbial mat rip-ups mineralized by pyrite form wavy-crinkly laminae which are similar to those in shales of the Mesoproterozoic Belt Group, Montana, and in many Phanerozoic units[32]. The laminated seams are fine-grained. Their parallel laminations are defined by variable crystal size and by variations in the concentration of clay and organic matter. Scanning electron microscopy (SEM) analyses indicate that the pyrite contains small amounts of sphalerite, chalcopyrite and galena. These sulphides also occur in veins that cut across bedding. Some of the small pyrite grains contain Se, Pb and, rarely, As. These textural and mineralogic characteristics as well as the association of the pyrite with organic-rich shales suggest an early diagenetic origin for all or nearly all of the pyrite.

Isotopic data

Drill core samples were cut parallel to bedding, polished, and then analysed. Early diagenetic pyrite grains larger than 0.5 mm in polished thick sections were pre-fluorinated, and SF_6 analyte was prepared by the *in situ* KrF excimer laser photoablation technique[33]. The analyte was passed through a gas chromatograph, peaks from contaminants were vented, and analysis of the purified SF_6 was made on a ThermoFinnigan Mat-251 at the Geophysical Laboratory of the Carnegie Institution. On a $\delta^{33}S^*$ versus $\delta^{34}S^*$ diagram, the isotopic composition of sulphur in the Rooihoogte-Timeball Hill pyrites plots along or close to a line with slope 0.5114 that passes through the origin (Fig. 4; $\delta^{33}S^*$ and $\delta^{34}S^*$ are defined[34] as $\delta^x S^* = 1{,}000\ln([\delta^x S/1{,}000]+1)$, where x is 33 and 34, respectively). All of the data in Fig. 4 lie within (or are less than the analytical error from) the area defined by fractionation arrays with slopes ranging between 0.500 and 0.516, typical of mass-dependent fractionation processes[35]. This indicates that the data in Fig. 4 can be explained without invoking any MIF.

Values of $\Delta^{33}S_{ln}$ in Table 1 were calculated by means of the equation $\Delta^{33}S_{ln} = \delta^{33}S^* - (0.5138\,\delta^{34}S^*)$, where the slope 0.5138 is defined by more than 100 unpublished analyses done at the Geophysical Laboratory. All the values are ≤0.33‰. This indicates that the range of the MIF signal in these data, if present at all, is much smaller than the range observed in most Archaean sulphides and sulphates but is similar to $\Delta^{33}S_{ln}$ values in recent marine barite[20].

Implication for the rise of oxygen in the atmosphere

If the $\Delta^{33}S_{ln}$ values of our data set are representative of sedimentary sulphur during the deposition of the Timeball Hill and Rooihoogte formations, they are strong indications that the level of atmospheric O_2 was $>10^{-5}$ PAL. The lack of MIF >0.33‰ could be related to a hydrothermal source of sulphur that was not influenced by photodissociation in the atmosphere, or to local, complete mixing of S species affected by MIF. However, the highly negative $\delta^{34}S$ values of sulphur in the pyrite, consistently small $\Delta^{33}S$ values over the 3.5-m-thick section of organic-rich shales, and their deposition in a shallow-water epicontinental basin far from sites of contemporaneous volcanic activity, speaks for its origin via the bacterial reduction of normal seawater sulphate.

Two additional observations support the interpretation that the lack of (or small) MIF signal in the Rooihoogte and Timeball Hill pyrites is related to the rise of the atmospheric oxygen level before these units were deposited rather than to local, complete mixing of S species affected by MIF. First, the $\delta^{34}S$ values of the pyrites range from −34.7 to −23.9‰. This range is consistent with the results of whole rock analyses in a previous study[26], suggesting that ^{34}S depletion in pyrites from these units is basin-wide. These values are much lower than those found in all older sedimentary units[13]. The small S isotope fractionation in the Archaean ocean has been explained by a seawater sulphate content of <200 μM (ref. 7). The Timeball Hill and Rooihoogte S isotope data suggest a higher seawater sulphate content during their deposition, consistent with an intensification of the oxidative part of the S cycle rather than local hydrothermal influence. Second, sandstones overlying shales of the lower Timeball Hill Formation contain iron ore consisting of haematitic oölites and pisolites deposited in shallow-water fluvial and deltaic settings[36]. These haematitic iron ores cover an area of >100,000 km^2 and contain ore reserves of 6 billion tons at 40–55% Fe (refs 36, 37). Their presence implies that the level of atmospheric oxygen was at least high enough to oxidize Fe in shallow deltaic and fluvial settings. These data are all consistent with an oxygen content of the atmosphere $>10^{-5}$ PAL.

Until recently, the age of the Rooihoogte and Timeball Hill formations was only constrained to be between 2.48 and 2.22 Gyr (Fig. 2). A Re–Os age of 2,322 ± 15 Myr has been reported[38] for the early diagenetic pyrites described above. The rise of atmospheric oxygen to values $>10^{-5}$ PAL therefore began before 2,322 ± 15 Myr ago. The Duitschland Formation, which is preserved in the north-eastern part of the Transvaal basin (Fig. 1), is a time equivalent of the Rooihoogte Formation. It occupies the same stratigraphic position with respect to the prominent underlying karstified unconformity

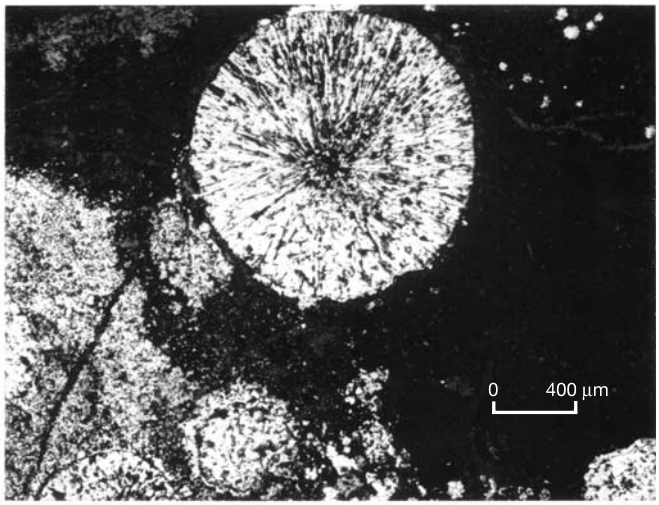

Figure 3 Reflected-light photomicrograph of pyrite spherulite in a polished thin section of sample EBA2/30-1.

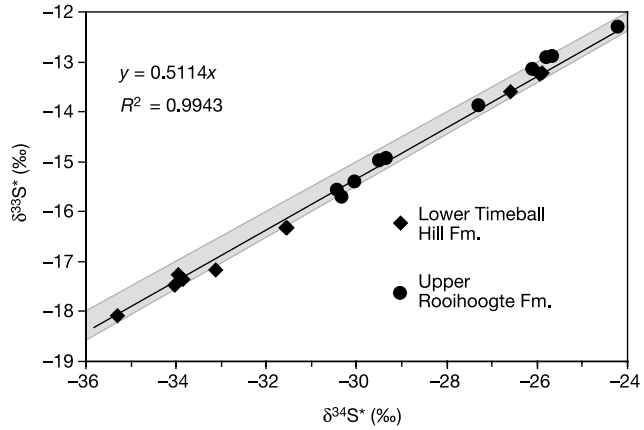

Figure 4 Plot of $\delta^{33}S^*$ versus $\delta^{34}S^*$ values in pyrite of the Rooihoogte and Timeball Hill formations. The grey area defines the field of isotopic data that can be produced by mass-dependent fractionation processes along the fractionation arrays with slopes ranging between 0.500 and 0.516 (ref. 35). Note that the $\delta^{33}S^*/\delta^{34}S^*$ ratio in the analysed samples lies on (or close to) the line of slope 0.5114.

©2004 Nature Publishing Group

surface and the overlying Timeball Hill Formation. There is a basal glacial diamictite in both the Duitschland and the Rooihoogte formations. Quartzites occur in the middle of both formations, and a chert breccia is present at their top[28]. The upper part of the Duitschland Formation contains marine carbonates with $\delta^{13}C$ values as high as +10.1‰, suggesting the production of excess oxygen by biological carbon cycling[39]. Their stratigraphic position is broadly correlative with that of the black shales of the Rooihoogte Formation, suggesting a possible link between the high relative burial rate of organic carbon and the rise of atmospheric oxygen.

There is still a time gap of ~150 Myr between the youngest sediments with a strong MIF signal (~2.47-Gyr-old Dales Gorge Member of the Brockman Iron Formation, Western Australia[18,40]) and the oldest sediments with a small or no MIF signal (Rooihoogte Formation). The record of sedimentation in the Huronian Supergroup, Canada might fill this gap. The glacial diamictites of the Rooihoogte and Timeball Hill formations have recently been correlated on the basis of chemostratigraphy and event stratigraphy with the second and third of the three glacial diamictites of the Huronian Supergroup, Canada[39]. Wing *et al.*[41]. found no $\Delta^{33}S$ values >0.3‰ in the sulphur isotopes of pyrite in shales that underlie and overlie the oldest glacial diamictite of the Huronian Supergroup in Ontario. This suggests that the loss of the MIF signal pre-dates the first glacial diamictite. However, the early diagenetic origin of the pyrite analysed by Wing *et al.* is not firmly established.

Although large MIF signals may have disappeared before the first glacial event, the O_2 content of the atmosphere seems to have remained very low until ~2,322 Myr ago. Detrital pyrite and uraninite grains occur in sandstones above the first glacial diamictite in North America[42] and pebbles of siderite facies iron formation occur in a conglomerate at the base of the Rooihoogte Formation[28]. The carbon isotope record, though still rather poorly defined for this time interval, does not indicate the presence of a positive excursion before the first glacial event or between the first and second glacial events[43]. The first major increase in atmospheric oxygen may, therefore, have occurred during the deposition of the Rooihoogte and Timeball Hill formations. □

Received 5 August; accepted 28 November 2003; doi:10.1038/nature02260.

1. MacGregor, A. M. The problem of the Precambrian atmosphere. *S. Afr. J. Sci.* **23,** 155–172 (1927).
2. Rasmussen, B. & Buick, R. Redox state of the Archean atmosphere: Evidence from detrital heavy minerals in ca. 3250–2750 Ma sandstones from the Pilbara Craton, Australia. *Geology* **27,** 115–118 (1999).
3. England, G. L., Rasmussen, B., Krapez, B. & Groves, D. I. Paleoenvironmental significance of rounded pyrite in siliciclastic sequences of the Late Archean Witwatersrand Basin: Oxygen-deficient atmosphere or hydrothermal alteration? *Sedimentology* **49,** 1133–1156 (2002).
4. Beukes, N. J. & Klein, C. Geochemistry and sedimentology of a facies transition—from microbanded to granular iron-formation—in the early Proterozoic Transvaal Supergroup, South Africa. *Precambr. Res.* **47,** 99–139 (1990).
5. Yang, W. & Holland, H. D. The redox-sensitive trace elements, Mo, U, and Re in Precambrian carbonaceous shales: Indicators of the Great Oxidation Event. *Geol. Soc. Am. Abstr. Programs* **34,** 381 (2002).
6. Holland, H. D. in *Early Life on Earth* (ed. Bengston, S.) 237–244 (Columbia Univ. Press, New York, 1994).
7. Habicht, K. S., Gade, M., Thamdrup, B., Berg, P. & Canfield, D. E. Calibration of sulfate levels in the Archean Ocean. *Science* **298,** 2372–2374 (2002).
8. Chandler, F. W. Proterozoic redbed sequences of Canada. *Can. Geol. Surv. Bull.* **311** (1980).
9. Chandler, F. W. Diagenesis of sabkha-related, sulphate nodules in the Early Proterozoic Gordon Lake Formation, Ontario, Canada. *Carbon. Evapor.* **3,** 75–94 (1988).
10. El Tabakh, M., Grey, K., Pirajno, F. & Schreiber, B. C. Pseudomorphs after evaporitic minerals interbedded with 2.2 Ga stromatolites of the Yerriba basin, Western Australia: Origin and significance. *Geology* **27,** 871–874 (1999).
11. Beukes, N. J. & Klein, C. in *Proterozoic Biosphere* (eds Schopf, J. W. & Klein, C.) 147–151 (Cambridge Univ. Press, Cambridge, UK, 1992).
12. Rye, R. & Holland, H. D. Paleosols and the evolution of atmospheric oxygen: A critical review. *Am. J. Sci.* **298,** 621–672 (1998).
13. Strauss, H. in *Precambrian Sedimentary Environments: A Modern Approach to Ancient Depositional Systems* (eds Altermann, W. & Corcoran, P. L.) 67–105 (Blackwell Science, Oxford, 2002).
14. Dimroth, E. & Kimberley, M. M. Precambrian atmospheric oxygen: Evidence in the sedimentary distribution of carbon, sulfur, uranium, and iron. *Can. J. Earth Sci.* **13,** 1161–1185 (1976).
15. Clemmey, H. & Badham, N. Oxygen in the Precambrian atmosphere: An evaluation of the geological evidence. *Geology* **10,** 141–146 (1982).
16. Phillips, G. N., Myers, R. E. & Palmer, J. A. Problems with the placer model for Witwatersrand gold. *Geology* **15,** 1027–1030 (1987).
17. Ohmoto, H. Evidence in pre-2.2 Ga paleosols for the early evolution of the atmospheric oxygen and terrestrial biota. *Geology* **24,** 1135–1138 (1996).
18. Farquhar, J., Bao, H. & Thiemens, M. Atmospheric influence of Earth's earliest sulfur cycle. *Science* **289,** 756–758 (2000).
19. Ono, S. *et al.* New insights into Archean sulfur cycle from mass-independent sulfur isotope records from the Hamersley Basin, Australia. *Earth Planet. Sci. Lett* **213,** 15–30 (2003).
20. Farquhar, J. *et al.* Mass-independent sulfur of inclusions in diamond and sulfur recycling on early Earth. *Science* **298,** 2369–2372 (2002).
21. Farquhar, J., Savarino, J., Airieau, S. & Thiemens, M. H. Observation of wavelength-sensitive mass-independent sulfur isotope effects during SO_2 photolysis: Implications for the early atmosphere. *J. Geophys. Res.* **106,** 1–11 (2001).
22. Romero, A. B. & Thiemens, M. Mass-independent sulfur isotopic compositions in sulfate aerosols and surface sulfates derived from atmospheric deposition: Possible sources of the MI anomaly and implications for atmospheric chemistry. *Eos* **83(** Fall Meet. Suppl.), B71A–0731 (2002).
23. Pavlov, A. A. & Kasting, J. F. Mass-independent fractionation of sulfur isotopes in Archean sediments: Strong evidence for an anoxic Archean atmosphere. *Astrobiology* **2,** 27–41 (2002).
24. Martini, J. E. J. The fluorite deposits in the Dolomite Series of the Marico District, Transvaal, South Africa. *Econ. Geol.* **71,** 625–635 (1976).
25. Bau, M., Beukes, N. J. & Romer, R. L. Increase of oxygen in the Earth's atmosphere and hydrosphere between ~2.5 and ~2.4 Ga B.P. *Mineral. Mag. A* **62,** 127–128 (1998).
26. Cameron, E. M. Sulphate and sulphate reduction in early Precambrian oceans. *Nature* **296,** 145–148 (1982).
27. Eriksson, K. A. The Timeball Hill Formation—A fossil delta. *J. Sedim. Res.* **43,** 1046–1053 (1973).
28. Coetzee, L. L.. *Genetic Stratigraphy of the Paleoproterozoic Pretoria Group in the Western Transvaal* Thesis, Rand Afrikaans Univ. (2001).
29. Eriksson, P. G. & Recsko, B. F. F. Contourites associated with pelagic mudrocks and distal delta-fed turbidites in the Lower Proterozoic Timeball Hill Formation epeiric basin (Transvaal Supergroup), South Africa. *Sedim. Geol.* **120,** 319–335 (1998).
30. Visser, J. N. J. The Timeball Hill Formation at Pretoria—A prograding shore-line deposit. *Ann. Geol. Surv. (S. Afr.)* **9,** 115–118 (1971) (1971–72).
31. Visser, J. N. J. in *Earth's Pre-Pleistocene Glacial Record* (eds Hambrey, M. J. & Harland, W. B.) 180–184 (Cambridge Univ. Press, New York, 1981).
32. Schieber, J. Microbial mats in terrigenous clastics: The challenge of identification in the rock record. *Palaios* **14,** 3–12 (1999).
33. Hu, G., Rumble, D. & Wang, P.-L. An ultraviolet laser microprobe for *in situ* analysis of multi-sulfur isotopes and its use in measuring Archean sulfur isotope mass-independent anomalies. *Geochim. Cosmochim. Acta* **67,** 3101–3118 (2003).
34. Miller, M. F. Isotopic fractionation and the quantification of ^{17}O anomalies in the oxygen three-isotope system: An appraisal and geochemical significance. *Geochim. Cosmochim. Acta* **66,** 1881–1889 (2002).
35. Farquhar, J. *et al.* Multiple sulphur isotopic interpretations of biosynthetic pathways: Implications for biological signatures in the sulphur isotope record. *Geobiology* **1,** 27–36 (2003).
36. Beukes, N. J., Dorland, H. C. & Gutzmer, J. Pisolitic ironstone and ferricrete in the 2.22–2.4 Ga Timeball Hill Formation, Transvaal Supergroup: Implications for the history of atmospheric oxygen. *Geol. Soc. Am. Abstr. Programs* **34,** 283 (2002).
37. Schweigart, H. Genesis of the iron ores of the Pretoria Series, South Africa. *Econ. Geol.* **60,** 269–298 (1965).
38. Hannah, J. L., Stein, H. J., Bekker, A., Markey, R. J. & Holland, H. D. Chondritic initial $^{187}Os/^{188}Os$ in Paleoproterozoic shale (seawater) and the onset of oxidative weathering. *Geochim. Cosmochim. Acta* **67** (2003) A-34.
39. Bekker, A. *et al.* Chemostratigraphy of the Paleoproterozoic Duitschland Formation, South Africa: Implications for coupled climate change and carbon cycling. *Am. J. Sci.* **301,** 261–285 (2001).
40. Mojzsis, S. J., Coath, C. D., Greenwood, J. P., McKeegan, K. D. & Harrison, T. M. Mass-independent isotope effects in Archean (2.5 to 3.8 Ga) sedimentary sulfides determined by ion microprobe analysis. *Geochim. Cosmochim. Acta* **67,** 1635–1658 (2003).
41. Wing, B. A. *et al.* $\Delta^{33}S$, $\delta^{34}S$ and $\delta^{13}C$ constraints on the Paleoproterozoic atmosphere during the earliest Huronian glaciation. *Geochim. Cosmochim. Acta* **66,** A840 (2002).
42. Roscoe, S. M. in *Geology of Canadian Mineral Deposit Types* (eds Eckstrand, O. R., Sinclair, W. D. & Thorpe, R. I.) P-1 10–23 (Geological Society of America, Denver, 1996).
43. Bekker, A. *et al.* Response of the exosphere to the 2.48–2.45 Ga superplume event. *Geol. Soc. Am. Abstr. Programs* **32** (2000) A-135.
44. Pickard, A. L. SHRIMP U-Pb zircon ages for the Palaeoproterozoic Kuruman Iron Formation, Northern Cape Province, South Africa: Evidence for simultaneous BIF deposition on Kaapvaal and Pilbara Cratons. *Precambr. Res.* **125,** 275–315 (2003).

Acknowledgements We thank D. Lange for help with the SEM work; W. Yang for help with sample preparation; and J. Brouwer for giving us access to drill core EBA-2, which was drilled by Gold Fields Ltd in the Potchefstroom area, and is now stored by the Geological Survey of South Africa. This study was supported by the NASA-Ames Research Center, NASA, PRF/ACS, NSF and South African Research Foundation.

Competing interests statement The authors declare that they have no competing financial interests.

Correspondence and requests for materials should be addressed to A.B. (abekker@fas.harvard.edu).

©2004 Nature Publishing Group